

1 **Test**

2 **Alexander Beck¹, Jan Henneberger¹, and Ulrike Lohmann¹**

3 ¹Institute for Atmospheric and Climate Sciences, ETH Zurich, Zurich, Switzerland

4 **Key Points:**

- 5 • In-situ measurements of microphysical cloud properties with a holographic Imager
6 • Influence of in-situ cloud observations at mountain top stations by ground based ice
7 enhancement processes
8 •

9 **Abstract**

10 In-situ cloud observations at mountain top research station regularly measure an ice crys-
 11 tal number concentration orders of magnitudes higher than expected from measurements
 12 or simulations of ice nuclei. The source of the majority of the observed ice crystals still
 13 remains an enigma. Several studies suggest a strong influence of mountain top in-situ
 14 measurements by surface based ice enhancement process, e.g. blowing snow, hoar frost
 15 or riming on trees, rocks and the snow surface. In this case the relevance of in-situ ob-
 16 servations on mountain top stations end/or a possible impact of such a surface based ice
 17 enhancement process on orographic clouds has to be further investigated.

18 In this study we assess the influence of surface based ice enhancement processes
 19 on in-situ cloud observations at mountain top stations. Therefore, vertical profiles within
 20 a height of 10 m above the snow covered surface were observed at the Sonnblick Ob-
 21 servatory in the Hohen Tauern Region, Austria. Results show that the ice crystal num-
 22 ber concentration decreases by at least factor of 2 within a height interval of 7.5 m if the
 23 Sonnblick Observatory was in cloud. During a short time period when the Sonnblick Ob-
 24 servatory was not in cloud an ice crystal number concentration of several hundreds per
 25 liter was observed at a height of 2.5 m and decreased to 10 per liter within a height interval
 26 of 7.5 m at a wind speed of 10 m s^{-1} . These observations strongly suggest that mountain
 27 top in-situ measurements are highly influenced by surface based ice enhancement pro-
 28 cesses.

29 **1 Introduction**

30 The microphysical properties of orographic clouds, e.g. their phase composition and
 31 cloud processes are key parameters for the clouds lifetime, extent, as well as the inten-
 32 sity of precipitation they produce [Rotunno and Houze, 2007]. On the other hand these
 33 parameters influence the radiative properties of midlevel clouds in the temperature range
 34 between 0 to -35 °C. Compared to a purely liquid cloud in this temperature range an ice
 35 cloud reflects 17 W m^{-2} more radiation than a pure ice cloud [Lohmann, 2002]. A well
 36 representation of orographic clouds is therefore crucial for accurate weather predictions in
 37 alpine terrain and improved climate models.

38 Because our understanding of fundamental processes of especially orographic mixed-
 39 phase clouds is still limited [Baumgardner *et al.*, 2011], in-situ measurements are impor-
 40 tant and frequently conducted at mountain top research stations. Despite an improved
 41 understanding on the origin of ice crystals from nucleation (citation!!!!) as well as from
 42 secondary ice multiplication processes [Field *et al.*, 2017] the source of most of the ice
 43 crystals observed at mountain top stations remains an enigma (citation!!!!). A study at
 44 the Elk Mountain reports ice crystal number concentrations on the order of several hun-
 45 dreds per liter close to the surface which was three orders of magnitude higher than ob-
 46 served on an aircraft aloft [Rogers and Vali, 1987]. Secondary ice multiplication processes
 47 like fragmentation [Rangno and Hobbs, 2001] or the Hallett-Mossop process [Hallet and
 48 Mossop, 1974] were ruled out by the authors due to the lack of large ice crystals, respec-
 49 tively large cloud droplets. Instead they proposed blowing snow as a surface based ice
 50 crystal source to generate such enormous ice crystal number concentrations near the snow
 51 surface. Ice crystal number concentrations in the order of 1000 per liter were also ob-
 52 served near the surface on the Antarctica Peninsula [Lachlan-Cope *et al.*, 2001]. They
 53 used formvar replica collected at a height of 2 m above the surface measure ice crystal
 54 number concentrations and suggested that the ice crystals originate from the snow covered
 55 surface. Lloyd *et al.* [2015] reported ice crystal number concentrations of up to 2000 per
 56 liter during the INUPIAQ project in February 2014 at the Jungfraujoch, Switzerland. They
 57 also ruled out secondary ice multiplication mechanisms as a possible source of these enor-
 58 mous ice crystal number concentrations. However, they also ruled out blowing snow as
 59 the source for ice crystal number concentrations larger than 100 per liter, because no cor-

60 relation of the ice crystal number concentration with wind speed was observed. Instead,
 61 they suggested hoar frost as a wind independent, surface based ice multiplication process
 62 to cause such high ice crystal number concentrations. Although these studies use different
 63 mechanisms to explain their measured ice crystal number concentration, they agree on an
 64 strong influence by surface based processes.

65 While the influence of mountain top measurements by surface based processes is
 66 widely accepted, the impact of the resuspended ice crystals on the development of a super-
 67 cooled orographic cloud, e.g. a more rapid glaciation and enhanced precipitation has not
 68 been studied extensively [Geerts *et al.*, 2015]. The properties of blowing snow have been
 69 studied in the context of snow redistribution ("snow drift") and reduced visibility due to
 70 the resuspended ice crystals. Usually the properties of the ice crystals were observed up to
 71 several meters above the snow surface Schmidt [1982]; Nishimura and Nemoto [2005]. It
 72 has been reported that blowing snow occurs above a wind speed threshold that varies be-
 73 tween 4 m s^{-1} and 13 m s^{-1} [Bromwich, 1988; Li and Pomeroy, 1997; Mahesh *et al.*, 2003;
 74 Déry and Yau, 1999]. Other than wind speed the concentration of blowing snow is con-
 75 trolled by snowpack properties (type of snow that fell, temperature and humidity of the
 76 snow pack, solar radiation and tree shadows) and atmospheric conditions (temperature,)
 77 [Vionnet *et al.*, 2013]. Schmidt [1982] observed that the ice crystal concentration decreases
 78 within one meter above the surface with the power of -0.5 to -1.1. Nishimura and Nemoto
 79 [2005] extended these measurements to a height of 9.6 m. They found that the ice crystal
 80 concentration usually decreases to as low as 1-10 particles per liter at a height of 9.6 m
 81 and the relative importance of the small ice crystals below $< 100 \mu\text{m}$ during a precipi-
 82 tation event decreases from nearly 100 % at 1.1 m to below 20 % at 9.6 m. With a rapid
 83 decrease in the ice crystals number concentration observed by these studies the impact
 84 of blowing snow on orographic clouds may be limited. However, most of these studies
 85 were conducted in dry air conditions where ice crystals undergo rapid sublimation [Yang
 86 and Yau, 2008], which may limit the applicability of these results. For hoar frost only one
 87 modeling study exists to our knowledge. Farrington *et al.* [2015] implemented a flux of
 88 surface hoar crystals in the WRF model based on a frost flower aerosol flux to simulate
 89 ice crystal concentrations measured at the Jungfraujoch by ?. They also found, that the
 90 surface ice crystals are not advected high into the atmosphere, limiting their impact on
 91 orographic clouds. They also suggest that more measurements on the ice crystal flux from
 92 the snow covered surface are necessary to simulate the impact of surface based ice crystal
 93 enhancement processes on the development of orographic clouds.

94 In contrast to these finding are several remote sensing studies exist, which suggest an
 95 influence by ice crystals advected from the surface as high as 1 km into the atmosphere.
 96 Satellite observations of Blowing Snow from MODIS and CALIOP exist over the Antarc-
 97 tica [?]. They observed layer thicknesses up to 1 km with an average thickness of 120 m
 98 for all observed blowing snow events. Similar observations from lidar measurements exist
 99 from the South Pole with an observed layer thickness of ice crystals of usually less than
 100 400 m [Mahesh *et al.*, 2003] and some rare cases when a subvisual layer exceeded a height
 101 of 1 km. However, a possible suspension of clear-sky precipitation could not be ruled out
 102 as a source of the observed ice crystal layers. Observations of layers of ice crystals also
 103 exist from radar measurements on an aircraft in the vicinity of the Medicine Bow Moun-
 104 tains [Vali *et al.*, 2012]. The observed ground-layer snow clouds were most of the time not
 105 visually detectable but produced a radar signal. Possible origin of ice crystals producing
 106 such ground-layer snow clouds are resuspended ice crystals from the surface or riming of
 107 cloud droplets at the surface. Geerts *et al.* [2015] presented evidence for ice crystals be-
 108 coming lofted up to 250 m in the atmosphere by boundary layer separation behind terrain
 109 crests and by hydraulic jumps. They also found evidence that ice crystals from the surface
 110 may lead to the glaciation of supercooled orographic clouds and enhanced precipitation.
 111 However, Geerts *et al.* [2015] also mention the limitation of radar and lidar measurement
 112 to separate the small ice crystals produced by surface processes from the larger falling
 113 snow particles and more abundant cloud droplets. They even suggest "to explore BIP

114 lofting into orographic clouds, ice particle imaging devices need to be installed on a tall
 115 tower, or on a very steep mountain like the Jungfraujoch".

116 In this study we assess the impact of surface based ice enhancement process, e.g.
 117 blowing snow or hoar frost on in-situ cloud observations at mountain top stations and a
 118 possible influence of orographic mixed-phase clouds. Therefore, for the first time, vertical
 119 profiles of surface based ice crystal production within a height of 10 m above the surface
 120 were observed in cloud at the Sonnblick Observatory.

121 This paper is structured as follows. The measurement site and set up of the field
 122 campaign are described in Section ???. The results are presented in section 3. In section
 123 4 the results are discussed and put in the context of earlier findings. A short summary is
 124 presented in section ???.

125 2 Field Measurements at the Sonnblick Observatory

126 2.1 Site description

127 This field campaign was conducted at the Sonnblick Observatory (SBO) situated at
 128 the summit of Mt. Sonnblick at 3106 masl (12°57'E, 47°3'N) in the Hohen Tauern Na-
 129 tional Park in the Austrian Alps. The SBO is a meteorological observatory operated all
 130 year by the ZAMG (Central Institute for Meteorology and Geodynamics). On the East and
 131 South the SBO is surrounded by large glacier fields with a moderate slope, whereas on the
 132 Northeast a steep wall of approximately 800 m descends to the valley (Fig. 1, right). Part
 133 of the SBO is a 15 m high tower used for meteorological measurements by the ZAMG.
 134 The data presented in this paper was collected during a field campaign in February 2017.

135 2.2 Instrumentation

136 The microphysical properties of clouds, hydrometeors and resuspended particles
 137 from the surface were observed with the HoloGondel platform [Beck *et al.*, 2017]. For
 138 this, the HoloGondel platform was mounted on an elevator that was attached to the me-
 139 teorological tower of the SBO (Fig. 2) to obtain vertical profiles of the microphysical
 140 properties within a height interval of 12 m above the surface where the platform was re-
 141 peatedly positioned at five different heights as indicated in Figure 2. On the Elevator the
 142 HoloGondel platform had a distance of approximately 1.5 m from the tower and was ori-
 143 ented in a way that the sampled air with the holographic imager HOLIMO 3G, which
 144 is the main part of the HoloGondel platform, was undisturbed during North and South
 145 wind cases. HOLIMO 3G captures the information of a three-dimensional volume of air
 146 containing cloud particles on a single image with a sample area of 20 mm x 13.4 mm.
 147 In this study the examined volume has a depth of 60 mm along the optical axis result-
 148 ing in a sample volume of 16 cm³. The open source software HoloSuite [Fugal, 2017]
 149 is used to reconstruct the in-focus images of the particles. Particles smaller than 25 µm
 150 are classified as liquid droplets, whereas particles larger than 25 µm are separated in liq-
 151 uid droplets and ice crystals based on the shape of their 2D image. Similar to a study by
 152 Schlenzeck and Fugal [2017] the ice crystals were further visually classified into three dif-
 153 ferent groups: regular, irregular and aggregates. Because the visual classification of sev-
 154 eral thousands of ice crystals is time consuming. this subclassification of ice crystals was
 155 done only for the profiles on February 17th.

156 Meteorological data are available from the measurements by the ZAMG and the
 157 HoloGondel platform. The ZAMG measures one minute averages of temperature, rela-
 158 tive humidity and horizontal wind speed and direction at the top of the meteorological
 159 tower. Snow cover depth is daily manually observed by the operators of the SBO. Based
 160 on these measurements the change of the snow cover is calculated. However, this calcula-
 161 tion includes all the changes in the snow cover depth, e.g. snow drift, sublimation, melting

162 and fresh snow. Daily measurements of the total precipitation are available on the North
 163 and South side of the SBO. Information about cloud base and cloud depth are available
 164 from a ceilometer which is located in the valley on the North of the SBO. An additional
 165 3D Sonic Anemometer, which is part of the HoloGondel platform, was mounted at the top
 166 of the meteorological tower. However, data is only available occasionally, because most of
 167 the time the heating of the Anemometer was not sufficient enough to prevent the build up
 168 of rime on the measurement arms.

169 3 Results

170 The data presented was observed on 4 February and 17 February 2017. Figure 3
 171 and 4 show an overview on the meteorological conditions on both days. The main differ-
 172 ence is the wind direction, which was South-West on 4 February and North on 17 Febru-
 173 ary.

174 3.1 4 February 2017

175 On 4 February a low pressure system moved eastwards from the Atlantic Ocean over
 176 northern France to western Germany, where it slowly dissipated. Influenced by this low
 177 pressure system the predominant wind direction at the Sonnblick was from Southwest
 178 on 4 February with wind speeds between 10 and 25 m s⁻¹. In the late afternoon around
 179 1900 UTC when the low pressure system dissipated over western Germany the wind di-
 180 rection changed to North at the Sonnblick and wind speeds decreased to a minimum of
 181 5 m s⁻¹. After 1900 UTC wind speed increased again to 15 m s⁻¹ at 2130 UTC. Starting
 182 from 0800 UTC the Sonnblick Observatory was in cloud except for a short time interval
 183 between 1910 and 2020 UTC. The temperature didn't change much during the day and
 184 stayed between -10 and -9 °C until 1900 UTC when the wind direction changed to North
 185 and the temperature slowly decreased to -11 °C at 22 UTC.

186 Between 0830 UTC and 2200 UTC a total total of 24 vertical profiles were obtained
 187 with the HoloGondel platform on the elevator attached to meteorological tower. No data
 188 is available from the CIP and the the 3D Sonic Anenometer. Therefore, only one minute
 189 averages of temperature, wind speed and direction are available from the ZAMG measure-
 190 ments (Fig. 3). Most of the profiles were obtained when the station was in cloud expect
 191 for four profiles between 1910 and 2020 UTC as indicated in Figure 3.

192 A summary of the 24 vertical profiles obtained on 4 February is shown in Figure 5.
 193 The ICNC reaches a maximum at 2.5 m above the surface. From this maximum the mean
 194 ICNC decreases by a factor of 2 and the median ICNC even by twice as much within a
 195 height interval of 7.5 m. These observations already suggest an influence of the measure-
 196 ments close to the snow surface by surface based ice crystal enhancement processes, but a
 197 rapid decrease with height.

198 Figure 6 shows a subset of 16 profiles representative for 4 February. The profiles
 199 are divided into 4 time periods representing different conditions during the day. The ver-
 200 tical profiles obtained in the time interval between 1910 and 2010 UTC, when the SOB
 201 was not in cloud, show a maximum in the vertical profile of the ICNC at 2.5 m. The max-
 202 imum ICNC at this height varies in between the four profiles and reaches up to 600 l⁻¹
 203 when the data is averaged over 50 holograms. The ICNC decreases with height for three
 204 of the profiles at least by a factor of 5 from an ICNC of more than 100 l⁻¹ at 2.5 m to
 205 less than 20 l⁻¹ at 10 m. This trend is well represented in the boxplot graph on the right
 206 of Figure 6. The mean ICNC of the data between 1910 and 2020 UTC averaged over 50
 207 holograms decreases from around 100 l⁻¹ at 2.5 m to 10 l⁻¹ at 10 m. The large extend of
 208 the shaded area represents the high variability of the ICNC even when the data is averaged
 209 over 50 holograms. Because the SBO was not in cloud during this time period, these mea-

surements strongly suggest an influence by surface based processes at a wind speed of less than 10 m s^{-1} of up to several hundreds of ice crystals per liter at a height of 2.5 m.

In the time period between 2030 and 2200 UTC, when the SBO was in cloud again, the vertical profiles shown in Figure 6 show a similar tendency. than before The maximum of the ICNC was observed at a height of 4.1 m and the ICNC decreases consistently for all four profiles with height above the observed maximum. The boxplot on the right of Figure 6 shows that the mean of the ICNC decreases by a factor of 9 from its maximum at 4.1 m to its minimum at 10 m. This decrease is in the same order of magnitude than in the cloud free case discussed above. If we assume that the observed ICNC at 10 m is representative for the cloud, the measurements at 2.5, 4.1 and 6.0 m are influenced by surface based processes and the magnitude of the influence is in the order of several hundreds of ice crystals per liter. This influence is in the same order of magnitude as it was observed between 1910 and 2020 UTC when the SBO was not in cloud. That the influence extends to a height of 6.0 m is probably due to an increased wind speed of up to 15 m s^{-1} .

The highest ICNCs were observed in the time period between 1200 and 1500 UTC (see Fig. 6 a) when also the wind speed reaches its maximum of 25 m s^{-1} . The summarized data of this time interval, which includes a total of 8 profiles shows an ICNC in the range of 300 to 700 l^{-1} with a maximum at 2.5 m and decreases by a factor of 2 within 7.5 m. The four profiles shown in Figure represent this trend, whereas the ICNC on an individual height varies by a factor of 2 between individual profiles. In this time interval the largest ICNCs and highest wind speeds were observed.

In the morning between 8300 and 1100 UTC the observed ICNC are much lower than between 1200 and 1500 UTC, although wind speed was as high as 20 m s^{-1} . Hier fehlt noch ein wenig Text...

For 4 February only 1 min averages of the wind speed and its maximum in the corresponding time interval are available from the SOB measurements (see Fig 3). To get an estimate of the correlation between wind speed and ICNC, the HoloGondel data was averaged over a timer interval of 1 min and compared to the maximum wind speed in the corresponding 1 min time interval, because it is expected that the gusts, i.e. the highest wind speed in an timer interval are most important for resuspending ice crystals from the surface. Figure 7 shows a clear trend between the maximum wind speed and ICNC. The ICNC increases by one order of magnitude between the lowest observed wind speed bin of $6\text{-}8 \text{ m s}^{-1}$ to the wind speed of $16\text{-}18 \text{ m s}^{-1}$. Only for the highest observed wind speed of $18\text{-}20 \text{ m s}^{-1}$ a decrease of the ICNC is observed.

3.2 17 February 2017

On 17 February a cold front over northern Europe was moving southwards causing mainly northerly flow across the alps and at the SBO. Wind speeds observed at the SBO in the time interval between 1800 and 2000 UTC were between 5 and 10 m s^{-1} (Fig. 4). In the same time interval temperature decreased by 1 K from -12.5 to -13.5°C . The SBO was in cloud starting from 1300 UTC with varying visibility between several meters up to several hundreds of meters. Some snow fall was observed in the afternoon between 1300 and 1500 UTC.

For this day wind data of the 3D Sonic Anemometer are available, which allow a more detailed analysis of the correlation between the observed ICNC and wind speed. Unfortunately, only four vertical profiles were obtained with the HoloGondel platform due to hardware problems with the computer of the platform. The first profile was measured in the morning at 1200 UTC when the SBO was not in cloud and no ice crystals were observed. Three more profiles were observed in the late afternoon starting from 1800 UTC. For these profiles the ice crystals have been classified by hand and subclassified in the three categories: regular, irregular and aggregates.

Figure 8 gives an overview on the three profiles observed in the late afternoon of 17 February. An ICNC of several hundreds was observed in the lowest height intervals with a maximum between 4.1 and 6.0 m. The minimal ICNC was consistently observed for all profiles at 10 m and was always below 150 l^{-1} . The decrease of the ICNC varies between a factor of 2 and 4. In general the observed profiles on this day are similar to the ones observed on 4 February between 2030 and 2200 UTC. This may be explained by very similar meteorological conditions. Wind direction was mainly from North to Northeast and wind speed varied between 5 and 10 m s^{-1} in both measurement intervals. Only temperature was slightly lower on 17 February.

In Figure 9 ICNCs are compared to various wind speeds. In contrast to the data of 4 February no correlation between ICNCs and the horizontal wind speed is observed. This holds true for the one minute average and maximum wind speed of the corresponding time interval observed by the SBO as well as the secondly average observed with the 3D Sonic Anemometer from the HoloGondel Platform. However, Figure 9c shows an increase of ICNC with the vertical wind speed.

All the ice crystals observed on 17 February were classified by hand a subclassification into irregular and regular ice crystals as well as aggregates was realized. The profiles of the subcategorized ICNCs and the relative abundance of these categories on the different heights are shown in Figure 10. ICNCs are dominated by irregular ice crystals, which is in good agreement with various other observations (citations). However, it is surprising to us that the relative importance of the irregular ice crystals stays constant with height or even increases. From surface based ice crystal enhancement processes irregular ice crystals are expected to enhance ICNCs near the surface. With increasing height this influence is expected to decrease and regular ice crystals to become more important. However, from this data a proportional decrease of the absolute number of regular and irregular ice crystals is observed. In Figure 11 the concentration of the different habits is correlated to the vertical wind speed observed. It is clearly visible that the ice crystal number concentration of irregular ice crystals show a stronger dependence on wind speed.

4 Discussion

correlation with wind speed: difficult to tell, because the time of measurement of a high ICNC and wind speed is not necessarily the time of the suspension of the ice crystals from the surface, secondly the amount of IC does not only depend on wind speed, but also on age of the snow cover, temperature.

5 Conclusion

Acronyms

SBO Sonnblick Observatory

Acknowledgments

Sonnblick Observatory and team (Elke Ludewig, Hermann Scheer, Norbert Daxbacher, Lug Rasser, Hias Daxbacher)

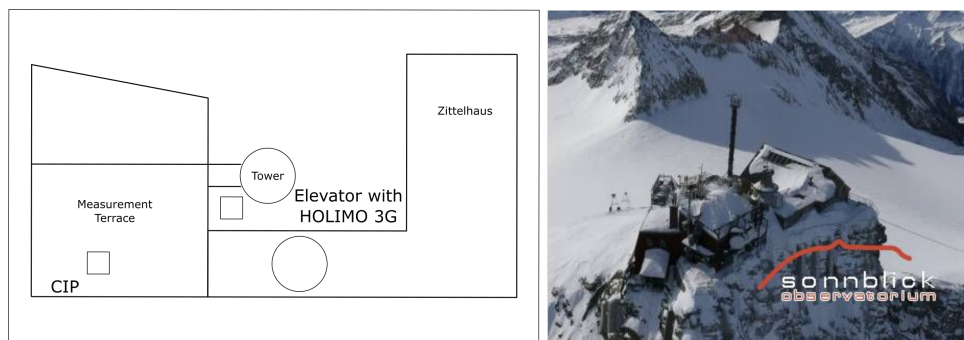
Thanks to Hannes, Olga, Fabiola, Monika, for their help

Thanks to Rob for many discussions

301 **References**

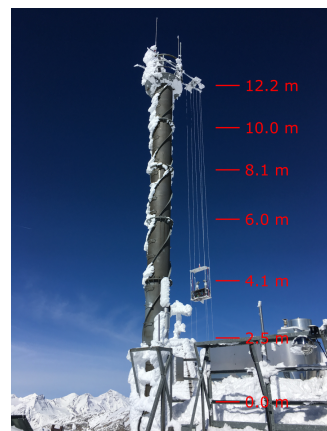
- 302 Baumgardner, D., J. Brenguier, A. Bucholtz, H. Coe, P. DeMott, T. Garrett, J. Gayet,
 303 M. Hermann, A. Heymsfield, A. Korolev, M. KrÃdmer, A. Petzold, W. Strapp,
 304 P. Pilewskie, J. Taylor, C. Twohy, M. Wendisch, W. Bachalo, and P. Chuang (2011),
 305 Airborne instruments to measure atmospheric aerosol particles, clouds and radiation:
 306 A cook's tour of mature and emerging technology, *Atmos. Res.*, 102(1â¬2), 10 – 29,
 307 doi:10.1016/j.atmosres.2011.06.021.
- 308 Beck, A., J. Henneberger, S. Schöpfer, J. Fugal, and U. Lohmann (2017), Hologondel, *At-*
 309 *mos. Meas. Tech.*
- 310 Bromwich, D. H. (1988), Snowfall in high southern latitudes, *Reviews of Geophysics*,
 311 26(1), 149–168, doi:10.1029/RG026i001p00149.
- 312 Déry, S. J., and M. K. Yau (1999), A climatology of adverse winter-type weather
 313 events, *Journal of Geophysical Research: Atmospheres*, 104(D14), 16,657–16,672, doi:
 314 10.1029/1999JD900158.
- 315 Farrington, R. J., P. J. Connolly, G. Lloyd, K. N. Bower, M. J. Flynn, M. W. Gallagher,
 316 P. R. Field, C. Dearden, and T. W. Choularton (2015), Comparing model and measured
 317 ice crystal concentrations in orographic clouds during the inupiaq campaign, *Atmos.*
 318 *Chem. and Phys.*, 15(18), 25,647–25,694, doi:10.5194/acpd-15-25647-2015.
- 319 Field, P. R., R. P. Lawson, P. R. A. Brown, G. Lloyd, C. Westbrook, D. Moisseev, A. Mil-
 320 tenberger, A. Nenes, A. Blyth, T. Choularton, P. Connolly, J. Buehl, J. Crosier, Z. Cui,
 321 C. Dearden, P. DeMott, A. Flossmann, A. Heymsfield, Y. Huang, H. Kalesse, Z. A.
 322 Kanji, A. Korolev, A. Kirchgaessner, S. Lasher-Trapp, T. Leisner, G. McFarquhar,
 323 V. Phillips, J. Stith, and S. Sullivan (2017), Secondary ice production: Current state of
 324 the science and recommendations for the future, *Meteorological Monographs*, 58, 7.1–
 325 7.20, doi:10.1175/AMSMONOGRAPHS-D-16-0014.1.
- 326 Fugal, J. P. (2017), Holosuite, in preparation.
- 327 Geerts, B., B. Pokharel, and D. a. R. Kristovich (2015), Blowing Snow as a Natural
 328 Glaciogenic Cloud Seeding Mechanism, *Mon. Weather Rev.*, 143(12), 5017–5033, doi:
 329 10.1175/MWR-D-15-0241.1.
- 330 Hallet, J., and S. Mossop (1974), Production of secondary ice particles during the riming
 331 process, *Nature*, 249, 26–28, doi:10.1038/249026a0.
- 332 Lachlan-Cope, T., R. Ladkin, J. Turner, and P. Davison (2001), Observations of cloud and
 333 precipitation particles on the avery plateau, antarctic peninsula, *Antarctic Science*, 13(3),
 334 339â¬348, doi:10.1017/S0954102001000475.
- 335 Li, L., and J. W. Pomeroy (1997), Estimates of threshold wind speeds for snow trans-
 336 port using meteorological data, *Journal of Applied Meteorology*, 36(3), 205–213, doi:
 337 10.1175/1520-0450(1997)036<0205:EOTWSF>2.0.CO;2.
- 338 Lloyd, G., T. W. Choularton, K. N. Bower, M. W. Gallagher, P. J. Connolly, M. Flynn,
 339 R. Farrington, J. Crosier, O. Schlenczek, J. Fugal, and J. Henneberger (2015), The ori-
 340 gins of ice crystals measured in mixed-phase clouds at the high-alpine site jungfraujoch,
 341 *Atmos. Chem. Phys.*, 15(22), 12,953–12,969, doi:10.5194/acp-15-12953-2015.
- 342 Lohmann, U. (2002), Possible aerosol effects on ice clouds via contact nucle-
 343 ation, *Journal of the Atmospheric Sciences*, 59(3), 647–656, doi:10.1175/1520-
 344 0469(2001)059<0647:PAEOIC>2.0.CO;2.
- 345 Mahesh, A., R. Eager, J. R. Campbell, and J. D. Spinhirne (2003), Observations of blow-
 346 ing snow at the south pole, *Journal of Geophysical Research: Atmospheres*, 108(D22),
 347 n/a–n/a, doi:10.1029/2002JD003327, 4707.
- 348 Nishimura, K., and M. Nemoto (2005), Blowing snow at mizuho station, antarctica, *Philo-*
 349 *sophical Transactions of the Royal Society of London A: Mathematical, Physical and En-*
 350 *gineering Sciences*, 363(1832), 1647–1662, doi:10.1098/rsta.2005.1599.
- 351 Rangno, A. L., and P. V. Hobbs (2001), Ice particles in stratiform clouds in the arctic and
 352 possible mechanisms for the production of high ice concentrations, *Journal of Geophysi-*
 353 *cal Research: Atmospheres*, 106(D14), 15,065–15,075, doi:10.1029/2000JD900286.

- 354 Rogers, D. C., and G. Vali (1987), Ice crystal production by mountain sur-
355 faces, *J. Clim. Appl. Meteorol.*, 26(9), 1152–1168, doi:10.1175/1520-
356 0450(1987)026<1152:ICPBMS>2.0.CO;2.
- 357 Rotunno, R., and R. A. Houze (2007), Lessons on orographic precipitation from the
358 mesoscale alpine programme, *Quarterly Journal of the Royal Meteorological Society*,
359 133(625), 811–830, doi:10.1002/qj.67.
- 360 Schlenzeck, O., and J. Fugal (2017), Microphysical properties of ice crystal precipitation
361 and surface-generated ice crystals in a high alpine environment in switzerland, *esult*, 56,
362 433–453, doi:10.1175/JAMC-D-16-0060.1.
- 363 Schmidt, R. A. (1982), Vertical profiles of wind speed, snow concentration, and
364 humidity in blowing snow, *Boundary-Layer Meteorology*, 23(2), 223–246, doi:
365 10.1007/BF00123299.
- 366 Vali, G., D. Leon, and J. R. Snider (2012), Ground-layer snow clouds, *Quarterly Journal*
367 *of the Royal Meteorological Society*, 138(667), 1507–1525, doi:10.1002/qj.1882.
- 368 Vionnet, V., G. Guyomarcâžh, F. N. Bouvet, E. Martin, Y. Durand, H. Bellot, C. Bel,
369 and P. Pugliažse (2013), Occurrence of blowing snow events at an alpine site over a
370 10-year period: Observations and modelling, *Advances in Water Resources*, 55, 53 – 63,
371 doi:<http://doi.org/10.1016/j.advwatres.2012.05.004>, snowâžAtmosphere Interactions
372 and Hydrological Consequences.
- 373 Yang, J., and M. K. Yau (2008), A new triple-moment blowing snow model, *Boundary-*
374 *Layer Meteorology*, 126(1), 137–155, doi:10.1007/s10546-007-9215-49.



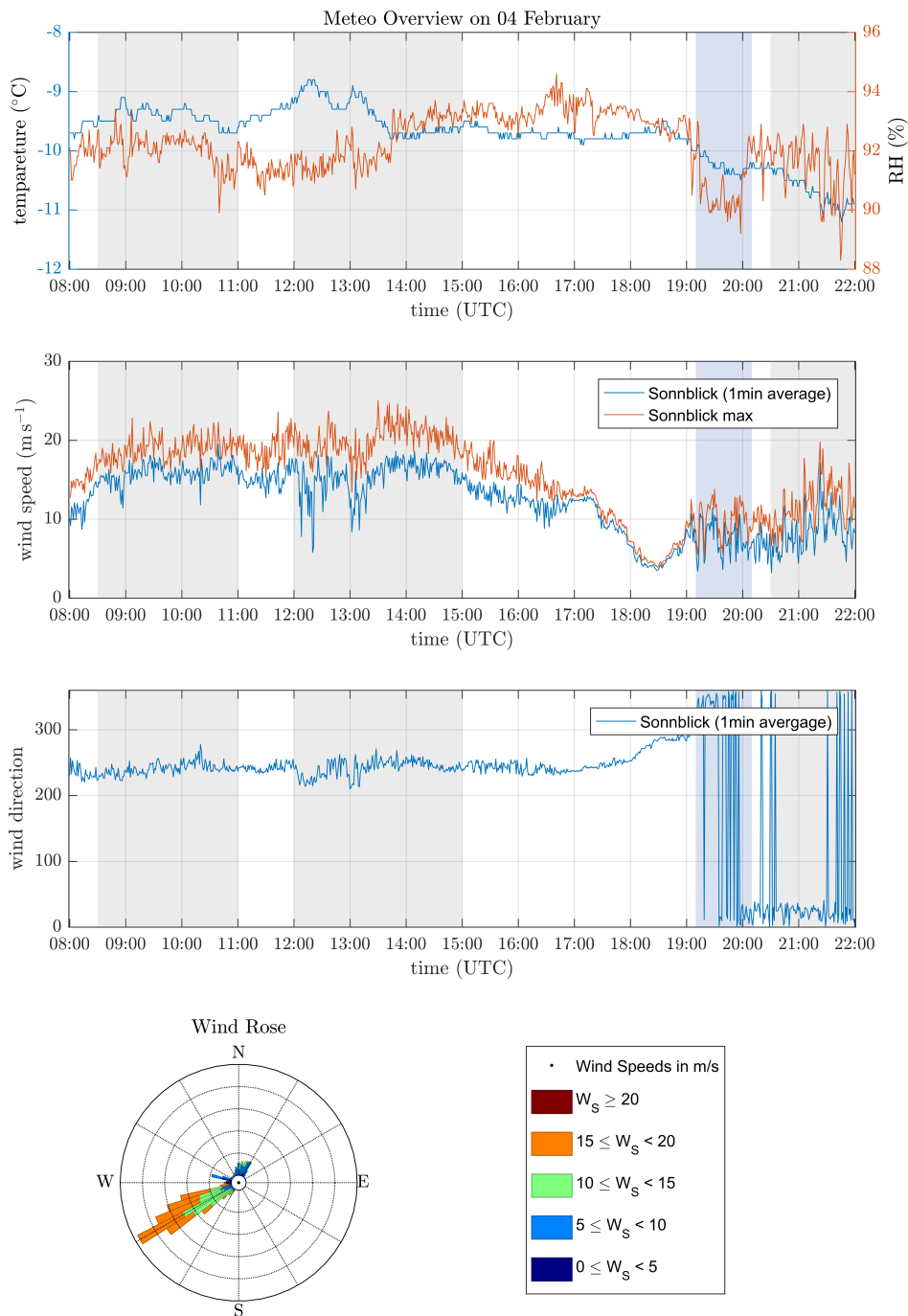
375

Figure 1. Short caption

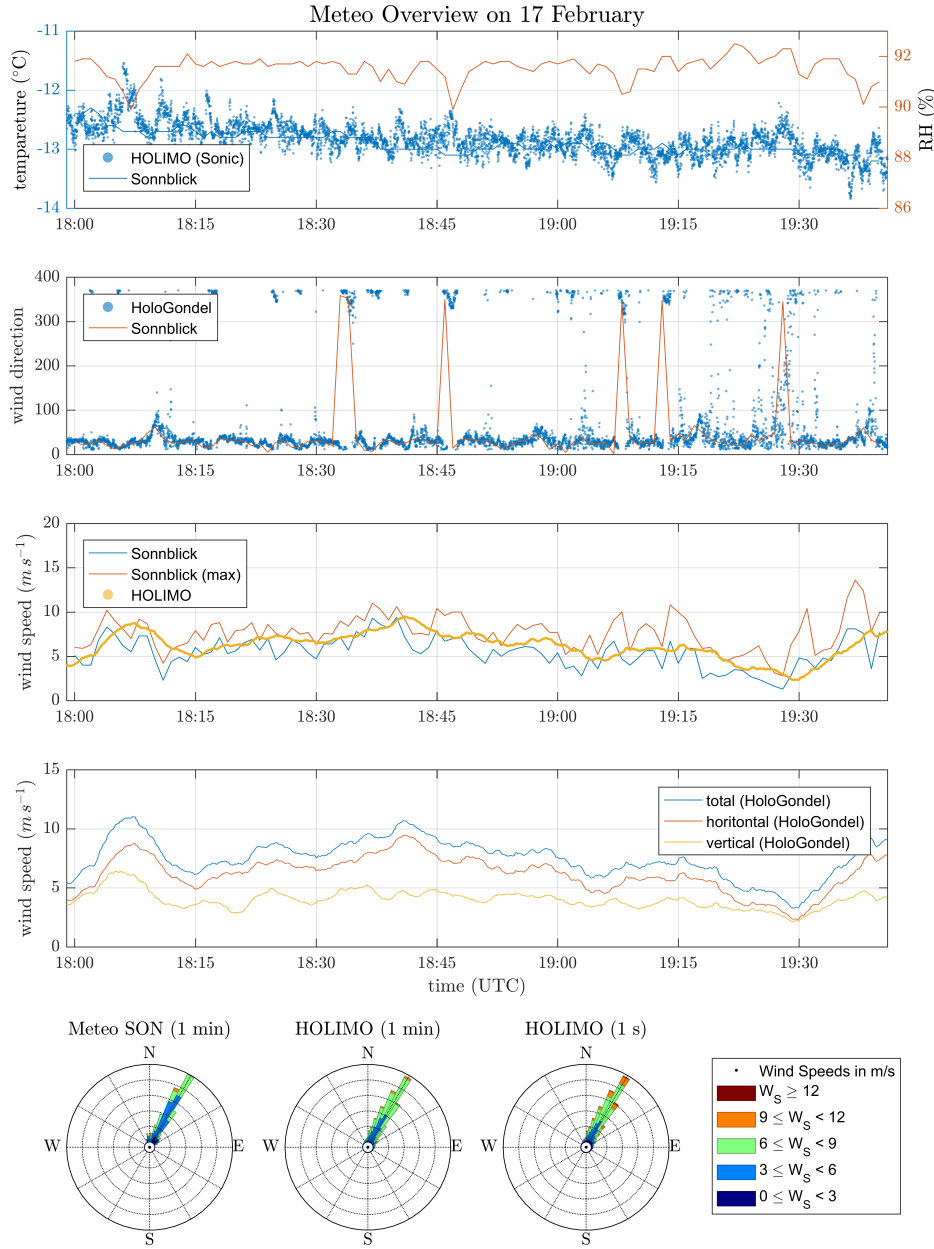


376

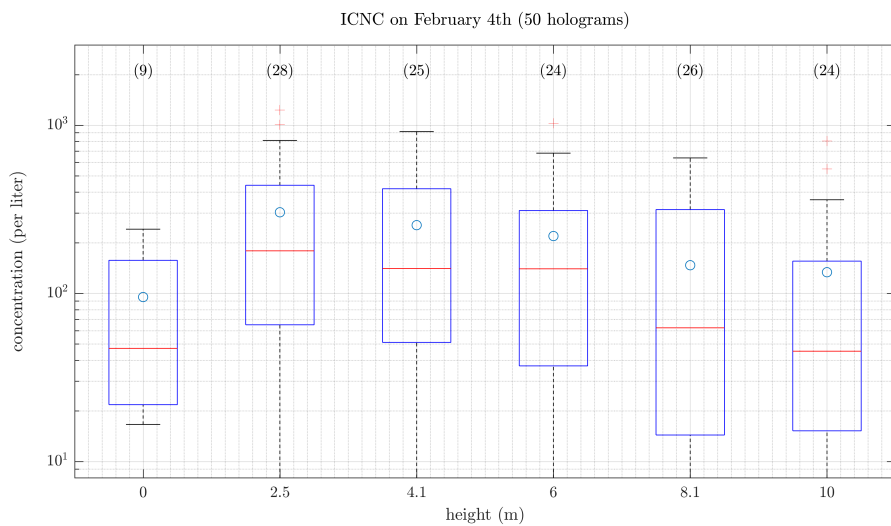
Figure 2. Short caption



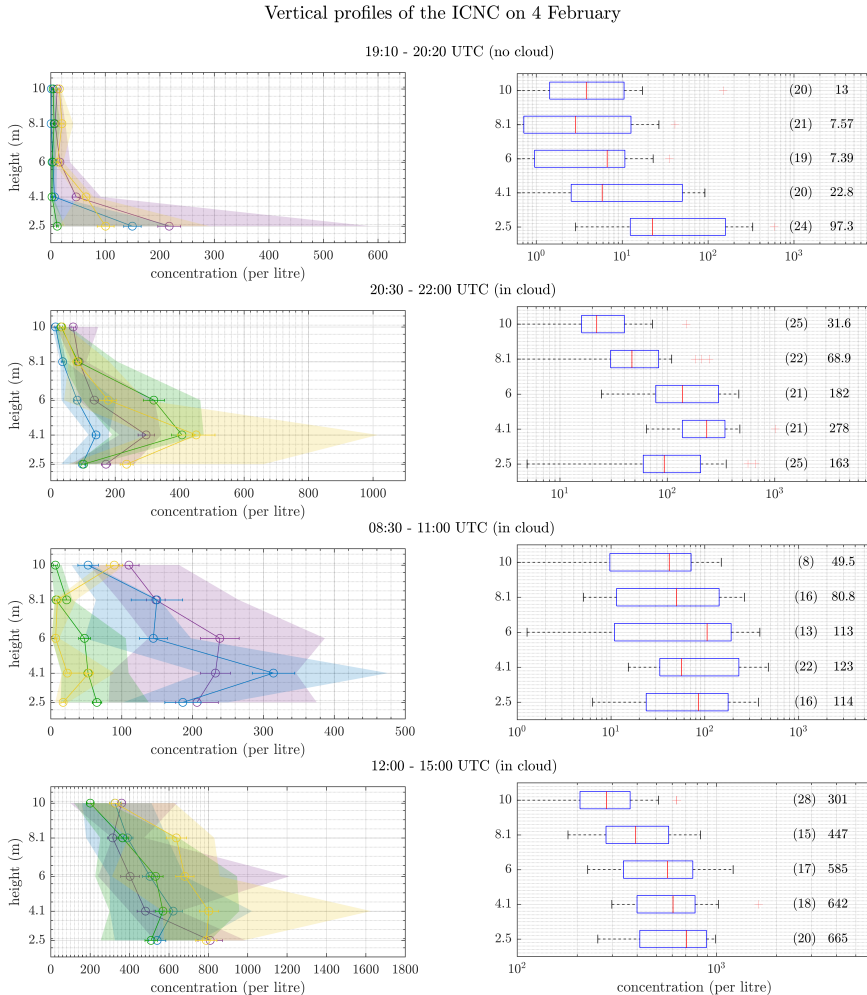
377 **Figure 3.** Overview of the meteorological conditions on 4 February obtained from the SBO measurements.
 378 Shown are the temperature, relative humidity (top), wind speed (second from top) and wind direction (second
 379 from bottom). All measurements are 1 m averages except for the maximum wind speed, which corresponds to
 380 the maximum wind speed observed during a corresponding 1 min average. A wind rose plot (bottom) of the
 381 wind measurement is also shown.



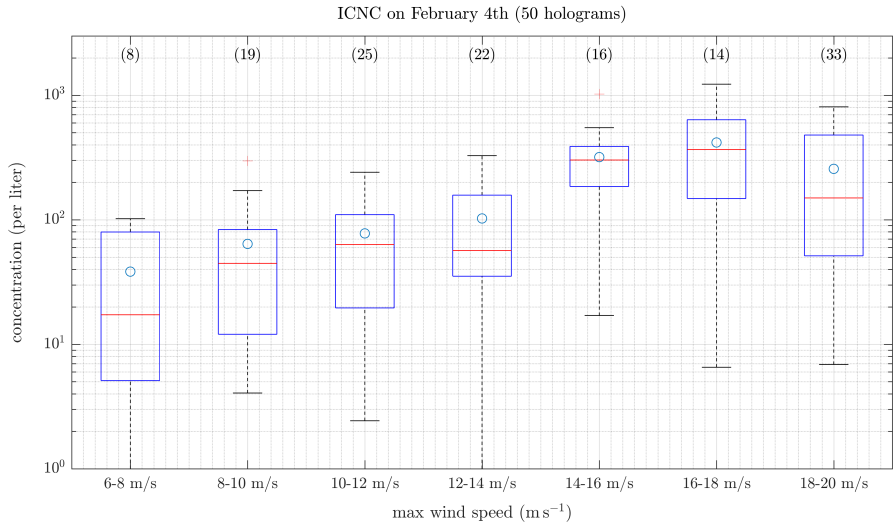
382 **Figure 4.** Overview on the meteorological conditions on 17 February. On this day temperature and wind
 383 measurements are available from the SBO and the HoloGondel platform. Shown are the temperature (Holo-
 384 Gondel and SBO), relative humidity (top), wind direction (second from top), a comparison of the horizontal
 385 wind speed (middle) and detailed wind speed measurements from the HoloGondel platform (second from bot-
 386 tom). A windrose plot is shown in the bottom panel. Wind measurements from the SBO and the HoloGondel
 387 platform agree well in direction and velocity.



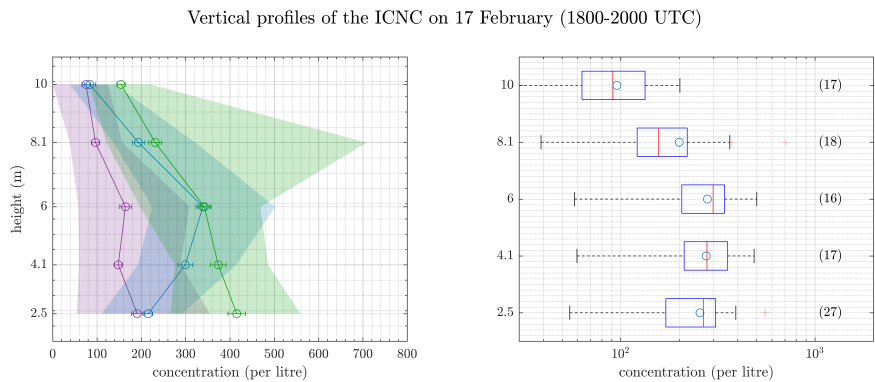
388 **Figure 5.** Ice crystal number concentration as a function of the height of the elevator at the meteorological
 389 tower of the SBO. This plot is a summary of the 24 profiles obtained on 4 February. The data was averaged
 390 over the entire time period of single measurements at the different height. The number in brackets is the
 391 number of measurements points, i.e. the number of measurements, at the different heights. For each box,
 392 the central line marks the median value of the measurement and the left and right edges of the box represent 25th
 393 and the 75th percentiles respectively. The whiskers extend to minimum and maximum of the data; outliers are
 394 marked as red pluses. The mean value of the measurements is indicated as a blue circle.



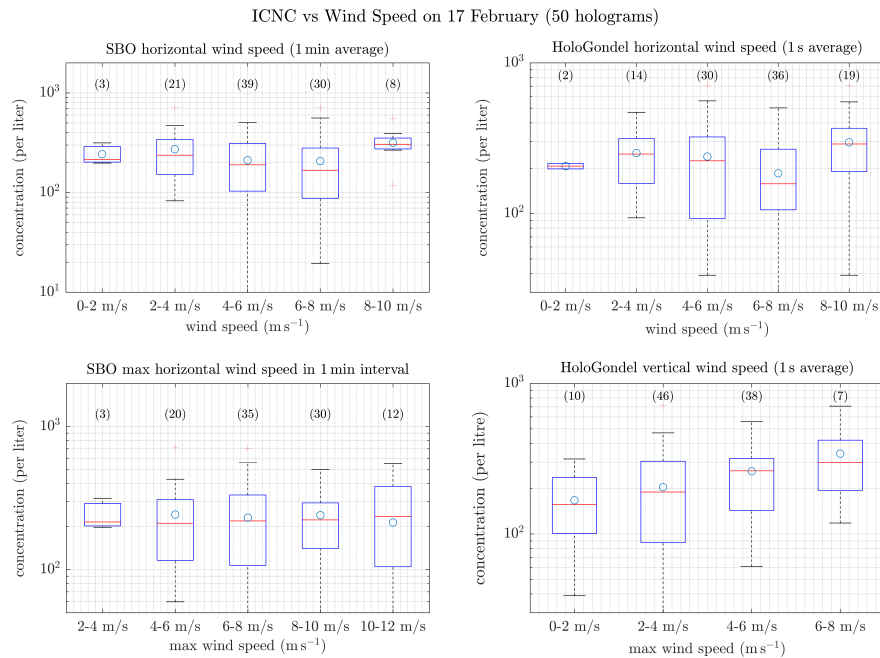
395 **Figure 6.** Ice crystal number concentration as a function of the height of the elevator at the meteorological
 396 tower of the SBO for four different timer intervals during 4 February, representing different meteorological
 397 conditions (Fig. 3). The individual profiles (left) are a representation for the different time intervals. The
 398 circles indicate the mean value averaged over the entire time interval. The error bars represent the standard
 399 error of the mean. The shaded area indicates the variability of the data and extends from the minimum to
 400 the maximum when the data is averaged over 50 holograms. For the summary of the different time intervals
 401 (right) the data is averaged over 50 holograms. For each box, the central line marks the median value of the
 402 measurement and the left and right edges of the box represent 25th and the 75th percentiles respectively. The
 403 whiskers extend to minimum and maximum of the data; outliers are marked as red pluses.



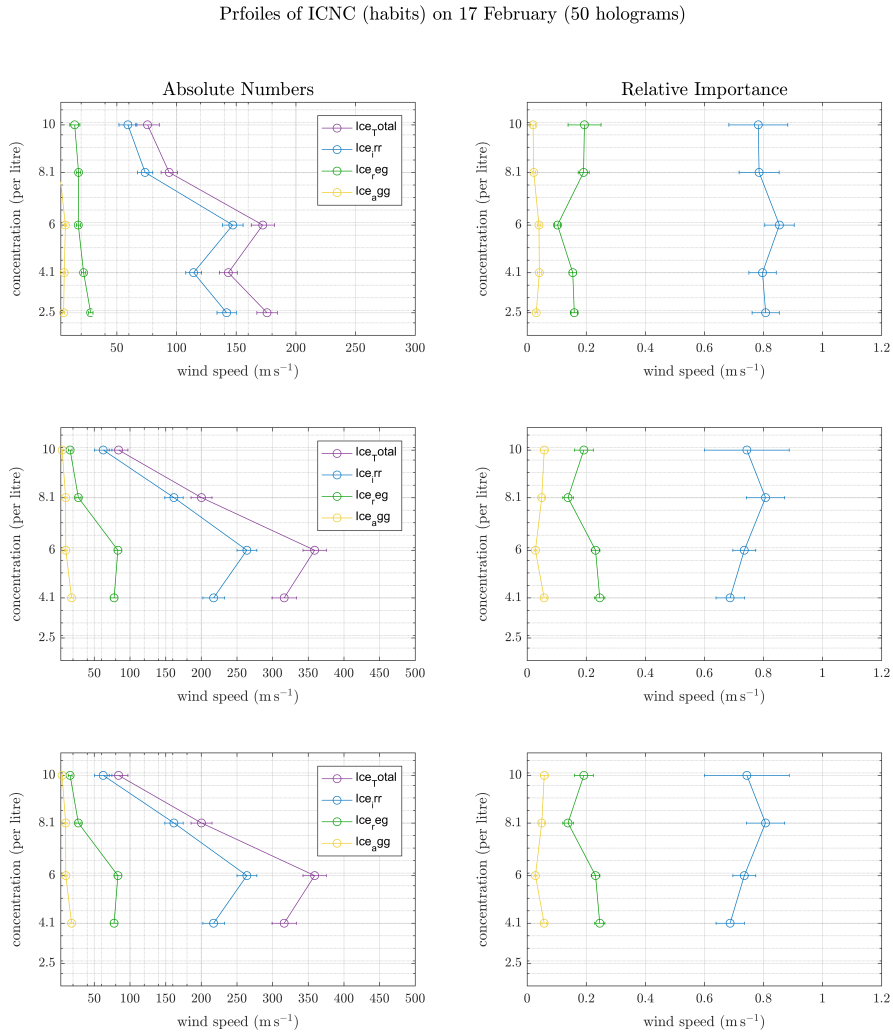
404 **Figure 7.** Ice crystal number concentration as a function of vertical wind speed. This plot is a summary of
 405 the entire data obtained on 4 February. The data was averaged over 50 holograms and categorized in 2 m s^{-1}
 406 wind speed intervals. The wind speeds are one minute averages from the SBO. The number in brackets is
 407 the number of measurements points, i.e. the number of measurements, obtained for the different wind speed
 408 intervals. For each box, the central line marks the median value of the measurement and the left and right
 409 edges of the box represent 25th and the 75th percentiles respectively. The whiskers extend to minimum and
 410 maximum of the data; outliers are marked as red pluses. The mean value of the measurements is indicated as
 411 a blue circle.



412 **Figure 8.** Ice crystal number concentration as a function of the height of the elevator at the meteorological
 413 tower of the SBO for 17 February. On the left are the three individual profiles obtained in cloud. The circles
 414 indicate the mean value averaged over the entire time interval. The error bars represent the standard error of
 415 the mean. The shaded area indicates the variability of the data and extends from the minimum to the maxi-
 416 mum when the data is averaged over 50 holograms. For the summary of the different time intervals (right) the
 417 data is averaged over 50 holograms. For each box, the central line marks the median value of the measurement
 418 and the left and right edges of the box represent 25th and the 75th percentiles respectively. The whiskers
 419 extend to minimum and maximum of the data; outliers are marked as red pluses.



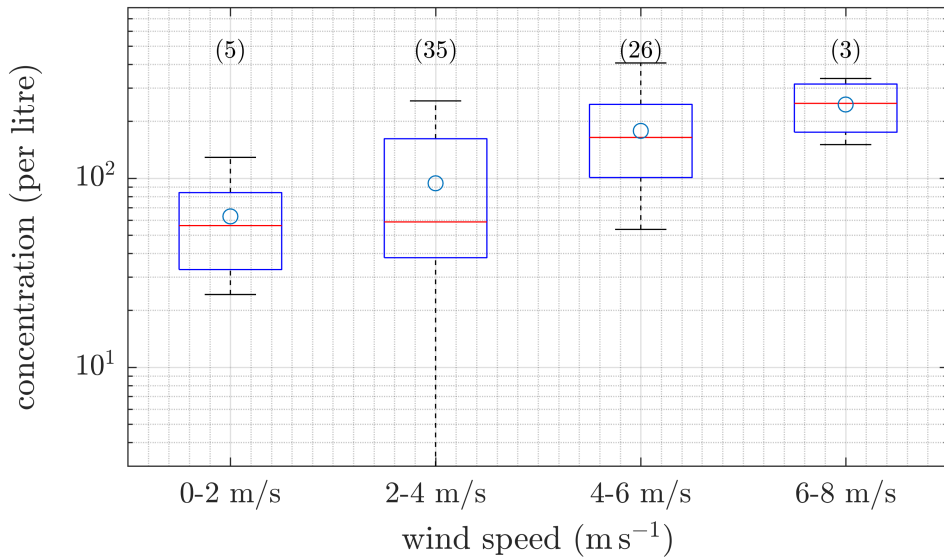
420 **Figure 9.** As Figure 7 only for 17 February and four different wind speed measurements: a) one minute
 421 b) maximum wind speed of the a corresponding time
 422 interval in a), c) secondly averages of the horizontal wind speed and d) secondly average of the vertical wind
 423 speed both from the 3D Sonic Anemometer.



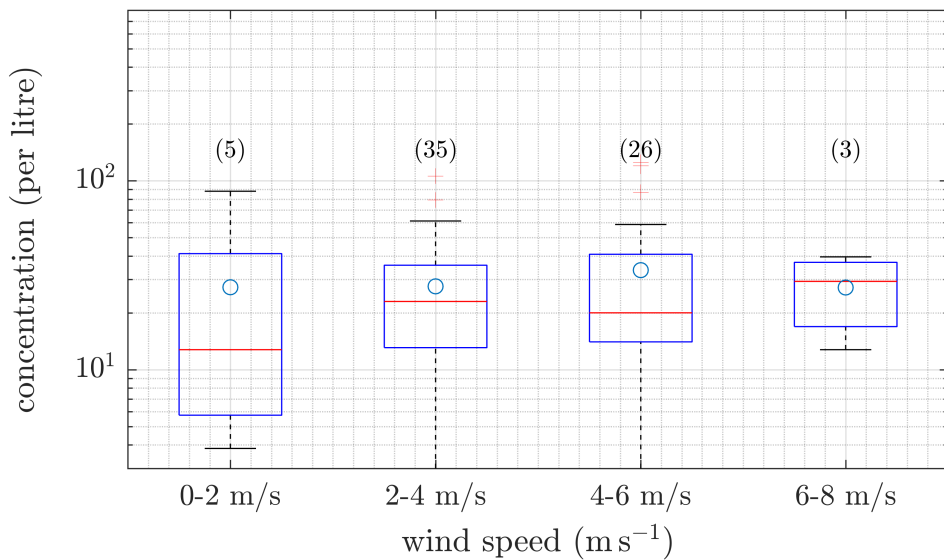
424 **Figure 10.** Vertical profiles of the concentration (left) and the relative importance (right) of the subclassified ice crystal habits: regular, irregular and aggregates. For the relative importance the number of ice crystals
 425 of different habits were divided by the total number of ice crystals. For theses plots the data as averaged
 426 over 50 holograms. In both cases the circles represent the mean of the 50 hologram averages. The error bars
 427 represent the standard error of the mean.
 428

ICNC (habits) vs Wind Speed on 17 February (50 holograms)

Irregular Ice Crystals



Regular Ice Crystals



⁴²⁹ **Figure 11.** As Figure 7 only for 17 February and different ice crystal habits as a function of the vertical
⁴³⁰ wind speed.